DOI 10.1007/s11182-017-1185-5

Russian Physics Journal, Vol. 60, No. 7, November, 2017 (Russian Original No. 7, July, 2017)

PLASMA PHYSICS

HETEROGENEOUS ARC DISCHARGE PLASMA IN A MAGNETIC FIELD

V. F. Myshkin,[1] M. Tichy,[1,2] V. A. Khan,[1,3] E. V. Bespala,[4] V. N. Lenskii,[1] and D. L. Gamov[1]

UDC 533.92; 539.196.5

Results of investigation of the plasma processes proceeding upon cooling of the heterogeneous low-temperature argon-oxygen arc discharge plasma in an external magnetic field are presented. The oxygen content is kept on the level insufficient for complete oxidation of carbon vapors. Upon cooling of the low-temperature plasma containing comparable amounts of C *and* Fe *atoms, the dispersed particles containing mixed microcrystals of carbon and iron oxides are formed. The particles formed from* Cu *and* SiO_2 *vapors in the arc discharge plasma are also studied. It is established that in the presence of the external magnetic field, the dispersed particles of mixed* C *and* Fe *or* Cu *and* SiO_2 *microcrystals have larger sizes than the particles formed in the absence of the magnetic field.*

Keywords: arc discharge, plasma chemistry, dispersed phase, carbon, iron vapors, magnetic field.

INTRODUCTION

Plasma processes are widely used for etchings, surface cleaning, coating deposition, nanotube production, and growing of diamond-like films. It is well known that the majority of chemical elements consist of two or more isotopes. The best physical and chemical parameters of solid state bodies are attained at definite proportions of the isotopes. Continuous expansion of the scope of isotope application is hampered by their high cost. Therefore, studies of the phenomena and processes aimed at reduction of the cost of isotope production are urgent. It has been demonstrated earlier that radical chemical processes in the low-temperature plasma are isotope-selective [1]. To reduce the isotope effect, it is necessary to separate the products of plasma processes enriched in isotopes from the initial substances for a short time, for example, based on different phase states [2].

The aim of this research is a study of a magnetic field effect on the processes proceeding in the argon-oxygen plasma containing C and Fe as well as Cu and SiO_2 atoms upon cooling. Section 1 of our work presents data on the equilibrium composition of the low-temperature plasma containing Fe, C, O_2, Ar, and N_2. Section 2 describes the magnetic field effect on the process of carbon plasma oxidation, and Section 3 considers a phase transition in the low-temperature plasma. Our experiment, its results, and discussion are presented in Sections 5, 6, and 7, respectively.

[1]National Research Tomsk Polytechnic University, Tomsk, Russia, e-mail: gos100@tpu.ru; vk@tpu.ru; gdl@tpu.ru; [2]Charles University, Prague, the Czech Republic, e-mail: milan.tichy@mff.cuni.cz; [3]V. E. Zuev Institute of Atmospheric Optics of the Siberian Branch of the Russian Academy of Sciences, Tomsk, Russia, e-mail: nt.centre@mail.ru; [4]JSC "Pilot and Demonstration Center for Uranium-Graphite Nuclear Reactors Decommissioning," Seversk, Russia, e-mail: bespala90@tpu.ru. Translated from Izvestiya Vysshikh Uchebnykh Zavedenii, Fizika, No. 7, pp. 17–25, July, 2017. Original article submitted December 7, 2016; revision submitted June 2, 2017.

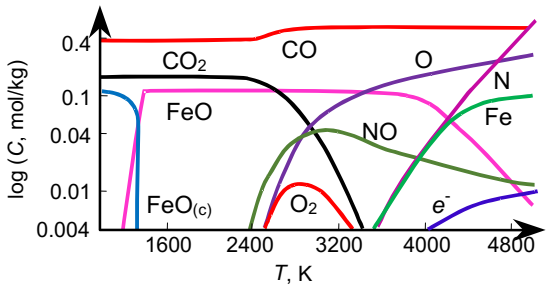

Fig. 1. Composition of the plasma containing Fe, C, N_2, O_2, and Ar as a function of the temperature.

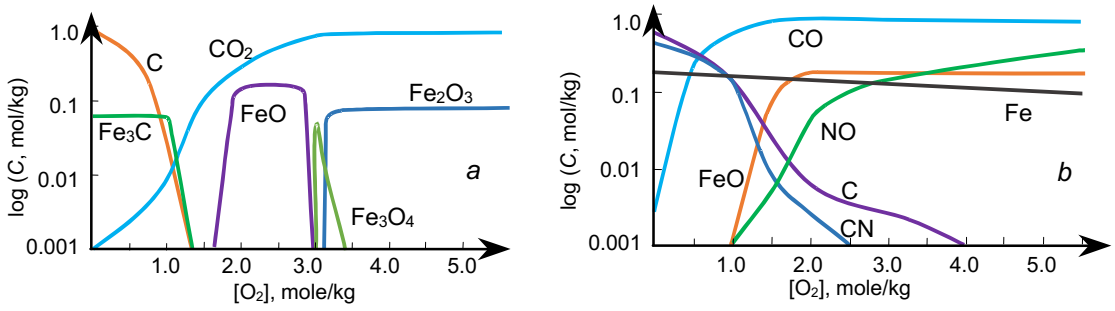

Fig. 2. Dependence of the maximum concentration of the compounds on the oxygen content in the plasma forming mixture at plasma temperatures 1000–1600 K (*a*) and 3500–5000 K (*b*).

1. CALCULATION OF THE EQUILIBRIUM COMPOSITION OF THE PLASMA CONTAINING FE, C, O_2, AR, AND N_2

It is well known that the temperatures of electrons and heavy particles in the arc discharge at atmospheric pressure differ insignificantly [3]. Therefore, it is possible to assume with a small error that the arc plasma at atmospheric pressure is in thermodynamic equilibrium. The initial mixture composition influences both physical and chemical processes and composition of end-products in plasma chemical processes [4]. To model the equilibrium plasma composition, we used the program complex *TERRA* [5]. A mixture of Ar, O_2, and N_2 at atmospheric pressure containing Fe and C atoms was considered as a plasma forming gas. Figure 1 shows the calculated equilibrium plasma composition at temperatures in the range 1000–5000 K for the Fe – 1 mol/kg, C – 1 mol/kg, O_2 – 2 mol/kg, Ar – 100 mol/kg, and N_2 – 50 mol/kg mixture. N_2 and Ar are not shown in Fig. 1.

The following regularities can be established based on the calculated results. CO_2 is formed only with an excess of oxygen compared to the stoichiometric value for Fe and C. The dispersed phase represented by the mixture of dispersed carbon and iron oxides is formed at low temperatures. Under conditions of thermodynamic equilibrium, dispersed carbon is formed in plasma forming mixtures (Ar – 100 mol/kg, Fe – 1 mol/kg, and C – 1 mol/kg) and (Ar – 70 mol/kg, Fe – 1 mol/kg, C – 1 mol/kg, and N_2 – 30 mol/kg) only at the oxygen content less than 1.3 mol/kg, and Fe_3C is formed at the O_2 content less than 1.5 mol/kg. The Fe_3C content at small oxygen content was 0.058 mol/kg and the dispersed carbon content was 1 mol/kg. The nitrogen, forming oxide at high temperatures, influenced insignificantly the amount of the dispersed phase formed in the plasma system.

The plots of the calculated content of the indicated compounds under the equilibrium conditions have maxima. The positions of the maxima on the temperature scale depend on the composition of the plasma forming mixture. Figure 2 shows plots of the dependence of the maximum content of the indicated compounds on the oxygen

concentration in the plasma forming gas mixture. The plots shown in Fig. 2*a* were calculated at temperatures in the range 1000–1600 K (the dispersed phase), and the plots shown in Fig. 2*b* were calculated at temperatures in the range 3500–5000 K (the gas phase). The amounts of CO and CO_2 gases increased with oxygen concentration in the mixture. The amount of formed dispersed carbon decreased with increasing oxygen content in the plasma forming mixture. At temperatures exceeding 3780 K, carbon was in the gas phase in the form of vapor. The CN concentration considerably decreased with increasing oxygen content. FeO, depending on the temperature, can be in the vapor or dispersed phase.

2. ISOTOPE SELECTIVITY OF PLASMA PROCESSES

It is well known that one of the conditions of forming a covalent chemical bond is Pauli's principle because of the law of conservation of spin during formation of the chemical bond [6]. The rate of chemical reaction in the gas phase is proportional to the ratio of the frequency of collision with formation of a molecule in the process of the first collision to the total frequency of collisions per unit volume. The external magnetic field leads to precession of spins of unpaired (valence) electrons of radicals. The probability of forming the CO molecule in the process of plasma oxidation of carbon isotopes in an external permanent magnetic field can be written as follows:

$$\delta = \sum_{i,j}^{n,m} \delta_{ij} \left[\mathrm{C}_i\right]\left[\mathrm{O}_j\right] \sigma_{ij}^{\mathrm{C-O}}\, \upsilon_{ij}^{\mathrm{C-O}} : \sum_{i,k}^{n,p} \left[\mathrm{C}_i\right]\left[X_k\right] \sigma_{ik}^{\mathrm{C}-X}\, \upsilon_{ik}^{\mathrm{C}-X}\,, \qquad (1)$$

where $[\mathrm{C}_i]$, $[\mathrm{O}_i]$, and $[X_i]$ are concentrations of carbon, oxygen, and plasma particles (including carbon and oxygen) with the *i*th velocity of thermal motion, $\sigma_{ij}^{\mathrm{C}-X}$ is the effective collision cross section of C and *X* radicals with relative velocity of motion $\upsilon_{ij}^{\mathrm{C}-X}$, δ_{ij} is the probability of forming singlet pair by valence electrons of colliding particles.

Without magnetic field, the isotope selectivity of plasma oxidation of carbon is determined by the known kinetic and thermodynamic factors. In the process of collisions in the magnetic field, only $1/(3n)$ fraction of collisions (singlet state) is completed by the formation of molecules as a result of thermal motion under conditions of thermodynamic equilibrium of the spin system, where *n* is the number of non-overlapping uncertainty ranges for the phase of spin precession in the range 360°. This quantity was estimated from the uncertainty ratio for the spin projections $\Delta S_x\, \Delta S_y \geq h/2 \mid \langle S_z \rangle \mid$. Therefore, for $\langle S_z \rangle = h/2$ with the dispersion $\Delta S_z = 0$, we obtain $\Delta S_x\, \Delta S_y \geq (h/2)^2$ [7]. In this case, the relaxation time of the spin system to the equilibrium state is much longer than the thermalization time of radicals with thermal velocities.

The efficiency of carbon isotope separation during plasma oxidation in a magnetic field is proportional to the ratio

$$\alpha = {}^{1}\delta : {}^{2}\delta\,, \qquad (2)$$

where ${}^{i}\delta$ is the probability of forming singlet pair in the process of collision of the *i*th isotope and the oxidizer. When analyzing the plasma processes in an external permanent magnetic field, it is necessary to consider the magnetic field of the arc that also affects the kinetics of physical and chemical processes during cooling of the vapor-gas mixture. The maximum magnetic field $B = \mu_0 I : (2\pi r)$ in the discharge channel with current *I* is formed on the surface of the plasma channel with radius *r* where phase transitions begin.

3. PROCESS OF PLASMA OXIDATION OF CARBON AND IRON ATOMS IN A MAGNETIC FIELD

The arc discharge channel contains atoms and ions of the plasma forming gas, vapors and ions of electrode materials, and electrode material in the form of droplets [8, 9]. Electrophysical reactions (of ionization of molecules and dispersed particles and recombination of charged particles) and chemical reactions run here. CO is formed at

temperatures in the range 9000–7000 K, and FeO is formed at temperatures less than 7000–5000 K. The latter condenses at temperatures in the range 1400–1600 K. In the presence of an excessive amount of oxygen, iron is oxidized to Fe_2O_3.

Because of the difference between concentrations of neutral components in the plasma channel and in the surrounding space, their radial diffusion takes place. The vapor-gas mixture is cooled in the region surrounding the discharge channel. This is accompanied by the formation of dispersed particles and their subsequent oxidation as well as by oxidation of vapors with formation of CO_2 and FeO_x molecules. The end products are largely determined by the rate of plasma cooling during its expansion. Oxidation of dispersed carbon is hampered by condensation of iron oxides on its surface. Therefore, retension of the proportion of carbon isotopes in different phase states formed in the plasma channel depends on the time of cooling from 3780 to 1400 K.

A large number of dispersed particles are formed in the arc discharge plasma. The rate of cooling of the vapor-gas mixture moving in the radial direction depends on the heat exchange processes. In the process of heat transfer, radiative heating and cooling of the vapor-gas mixture takes place at each point in the radial direction around the plasma channel. Convective heat transfer prevails along the vertical axis of the arc discharge. The formation and coagulation of dispersed particles leads to heating of the vapor-gas mixture.

Many interrelated elementary processes caused by collisions of neutral particles, ions, and electrons as well as by the absorption and emission of photons occur in the low-temperature electric discharge plasma containing several chemical compounds. These processes determine the rates of excitation (relaxation) of electronic, vibrational, and rotational levels, dissociation of molecules, and formation of molecules or particles of the dispersed phase.

The main chemical reactions that determine the parameters of the end products of the plasma processes are reactions of oxidation of carbon and iron atoms. The relative fraction of the residual atomic components largely determines their relative fractions in the condensed phase, and the frequency of forming condensation nuclei and the nucleation rate determine the dispersed particle size distribution.

At temperatures below 5000 K, iron oxidation is possible. Upon plasma cooling, the reaction of oxidation by molecular oxygen

$$Fe + O_2 \rightarrow FeO + O \tag{3}$$

prevails, which is characterized by the rate constant $k_2(T) = 1.6\cdot10^{-9}(T/298)^{-0.02}e^{-93322/RT}$ cm^3/(mol·s) at T = 200–2500 K [10]. With an excess of oxygen, the chemical reaction of the subsequent FeO oxidation is possible:

$$FeO + O_2 \rightarrow FeO_2 + O, \tag{4}$$

with the constant $k_3(T) = 1.02\cdot10^{-11}(T/298)^{0.40}e^{-68180/RT}$ cm^3/(mol·s) at T = 1000–3000 K [11]. Depending on the excitation energy and the multiplicities of the initial and final states, different scenarios of the above-indicated reactions are possible. For example, in the process of collision of the components $Fe(a^5F) + O_2(a^1\Delta_g)$ in the first electronically excited states, the following reactions are possible [12]:

$$Fe(a^5D_4) + O_2(a^1\Delta_g) \rightarrow FeO_2(^5A_1),\ \Delta H_0 = -376 \text{ kJ/mol}, \tag{5a}$$

$$\rightarrow Fe(a^5D_4) + O_2(X^3\Sigma_g),\ \Delta H_0 = -94 \text{ kJ/mol}, \tag{5b}$$

$$\rightarrow Fe(a^5F_5) + O_2(X^3\Sigma_g),\ \Delta H_0 = -10 \text{ kJ/mol}, \tag{5c}$$

$$\rightarrow FeO(^5\Sigma) + O(^3P),\ \Delta H_0 = (-2 \pm 20) \text{ kJ/mol}. \tag{5d}$$

Highly exothermic reactions (5a) are due to formation of the state with low level of electronic excitation [13]. The reaction between Fe in the ground state and O_2 ($X^3\Sigma_g$) has only one channel of forming FeO_2 with electron activation energy of ~17 kJ/mol [14].

The quasi-resonant electron energy transfer Fe (a^5F) + O_2 (X) is also possible. Depending on the multiplicity of Fe(a^5F), the heat in this reaction channel fluctuates from –10 to +4 kJ/mol. At temperatures below 7000 K, the reaction of carbon oxidation is possible:

$$C + O + M \rightarrow CO + M,$$

with the constant k_1(8000 K) = $2.0 \cdot 10^{-34}$ cm^3/(mol·s) [15]. For example, one of the dominating products of the reaction C ($^3P_4$) + O_2 ($X^3\Sigma_g$) will be vibrationally excited CO in the ground electronic state [16]:

$$C(^3P_4) + O_2(X^3\Sigma_g^-) \rightarrow CO(X^1\Sigma^+, v) + O(^3P),$$

which is possible due to sufficiently high reaction heat ΔH = –132.6 kJ/mol (5.75 eV) (the vibrational CO quantum is equal approximately to 0.26 eV).

As a result of an electron impact, electronically excited $O_2(a^1\Delta_g)$ and $O_2(b^1\Sigma_g^+)$ molecules in singlet states, vibrationally excited $O_2(X^3\Sigma_g^-, v)$ molecules, and atomic oxygen O(^{3}P) are formed in the electric discharge in the oxygen medium [17, 18]. Relative contributions of the above-indicated excited states were presented in [19] depending on the energy deposited per unit volume.

4. FORMATION OF THE CONDENSED PHASE UPON COOLING OF THE LOW-TEMPERATURE PLASMA

The graphite evaporation temperature is 3780 K, and the iron evaporation temperature is 3023 K. Iron oxide Fe_2O_3 (hematite) melts at 1912 K and decomposes with increasing temperature. The saturated iron vapor pressure at a temperature of 1900 K is 13.3 Pa, and the saturated carbon vapor pressure at 2030 K is 1.33 Pa. These data demonstrate that carbon desublimation can be considered homogeneous.

The formation of nucleation centers and dispersed particles in a multicomponent system begins from the component that has the lowest saturated vapor pressure under the given conditions. The growth of primary carbon particles is limited by their heating to the sublimation temperature (the specific heat of graphite evaporation is 50 000 kJ/kg) during the phase transition. Then coagulation of somewhat cooled carbon particles proceeds with a slower rate. The energy liberated in the process of forming agglomerates contributes to formation of particle with a homogeneous crystal structure. The dispersed carbon coagulation rate constants for various processes observed in a gas flow are presented in [20] at temperatures in the range 470–530°C.

The nucleation theory with formation of liquid droplets has well been developed. The energy of forming the neutral cluster whose surface can be clearly distinguished is [21, 22]

$$\Delta G_n = n\left(\mu_c - \mu_v\right) + 4\pi r^2(n)\sigma, \tag{6}$$

where n is the number of atoms in the cluster; μ_c and μ_v are the chemical potentials of vapor atoms in the condensed and gas phases, respectively; $r(n)$ is the radius of the cluster containing n atoms; and σ is the cluster surface tension coefficient. The rate of temperature change of the formed dispersed particle with time is determined by cooling and heating rates as a result of liberation of the energy of phase transition:

$$\frac{dT}{d\tau} = q\frac{dn}{d\tau}\frac{1}{m_d\, c}, \tag{7}$$

where n is the flow of vapor atoms on a dispersed particle, m_d is the dispersed particle mass, q is the vaporization heat per 1 atom [J/atom], and c is the specific heat of substance of the dispersed phase.

Cooling of the dispersed particles in the plasma is caused by losses on heat conductivity and Plank radiation. The radiative energy losses of the dispersed particles are

$$Q_R = \sigma_R \varepsilon(T, R) T^4, \tag{8}$$

where $\varepsilon(T, R)$ is the blackness coefficient and σ_R is the Stefan–Boltzmann coefficient. The period of frequency stabilization of the formation of nucleation centers depends on the temperature and is about 10^{-9} s [23]. From the theory of fluctuations it follows that the rate of forming the nucleation centers of the new phase in unit volume for unit time is

$$\frac{dN}{d\tau} = \frac{\gamma}{\rho}\sqrt{\frac{2m\sigma}{\pi}}\left(\frac{P}{kT}\right)^2 \exp\left(-\frac{\Delta G}{kT}\right), \tag{9}$$

where N is the numerical concentration of droplets, in cm^{-3}; τ is time, in s; $k = 1.38 \cdot 10^{-23}$ J/K is the Boltzmann constant; γ is the desublimation coefficient; m is the mass of the vapor molecule, in kg; T is the temperature of the mixture, in K; P is the total pressure of the vapor-gas mixture, in mm Hg; and ρ is the sublimate density [24]. The coefficient γ gives the relative fraction of vapor molecules remaining as a result of impacts on the solid surface; γ is in the range 0–1.

The surface energy σ of the solid dispersed particle can be determined from the equation [25]

$$\sigma = \frac{\Delta H - RT}{V^0}\frac{\Delta n}{n}h, \tag{10}$$

where ΔH is the entropy change during evaporation, in kJ/mol; $R = 8.314$ J/(mol·K) is the universal gas constant; n is the coordination number; Δn is the number of vacancies for atoms on the surface of the crystal lattice; h is the thickness of the monolayer of molecules, in m; $V^0 = M : \rho$ is the molar volume of the solid substance, in cm^3/mol; and M is the molar mass of the desublimate, in g/mol. The presence of charges on condensation nuclei (nucleation centers) facilitates formation of the new phase and promotes further microcrystal growth. Therefore, the sizes of critical nucleation centers in the low-temperature plasma significantly decrease.

It is well known that the phase transition in the low-temperature plasma is possible both on a colder surface and in the bulk [26, 27]. The formation of nucleation centers of the solid phase in the vapor volume upon its cooling begins when supersaturation exceeds its critical value S_{cr}. The formation of nucleation centers decreases supersaturation, which causes a significant decrease in the rate of forming the nucleation centers. Then the concentration of substance in the vapor phase decreases due to the increased sizes of the dispersed particles. The fast formation of dispersed particles from unreacted isotopes allows the kinetic isotopic effects of chemical reactions to be observed. In this case, the unreacted carbon goes into the dispersed phase and is isolated from oxygen with the help of iron oxides.

The supersaturation of vapors of the condensed phase can cause a nonequilibrium state of the cooling plasma. The volume condensation leads to the formation of finely dispersed particles that can affect the electron concentration and other plasma properties. This change is caused by the change of the electron concentration and the decrease of the electron mobility. The presence of particles in the condensed dispersed phase (CDF) in the low-temperature plasma changes the electronic gas density at the expense of the thermionic emission or the attachment of electrons. The formula for the dispersed particle charge distribution in the low-temperature charge-balanced plasma can be written as follows [28]:

$$\frac{N_{Z+1} N_e}{N_Z} = 2\left(\frac{m_e T_e}{2\pi\hbar^2}\right)^{3/2} \exp\left(-\frac{I}{T_e}\right), \tag{11}$$

where N_Z is the concentration of the dispersed particles with the charge Z, T_e and N_e is the temperature and concentration of electrons, m_e is the electron mass, I is the cluster ionization potential, and h is Planck's constant.

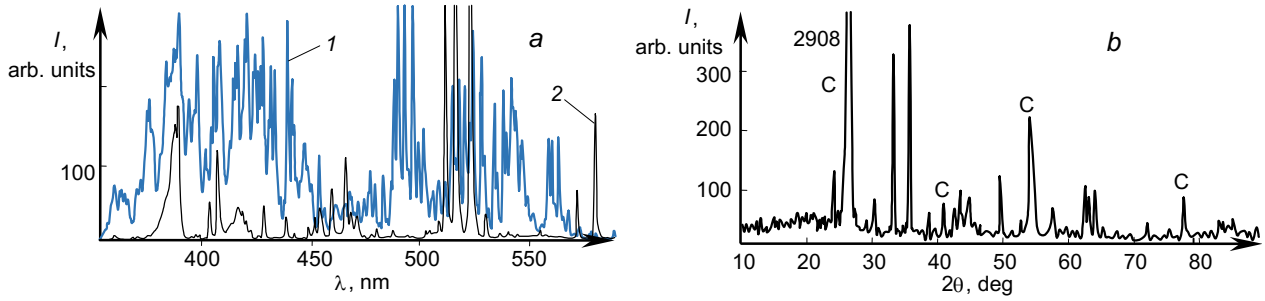

Fig. 3. Experimental data: *a*) arc discharge plasma spectrum and *b*) x-ray diffraction pattern of the powder formed by the arc discharge plasma (H = 0 mT).

The kinetics of the plasma with the CDP was considered in detail in [29]. It was shown that the time of electronic density relaxation to the equilibrium is determined by the time of dispersed particle charge relaxation rather than by the processes of atom ionization and electron and ion recombination.

5. EXPERIMENTAL SETUP

To study the influence of an external magnetic field on the plasma processes of forming particles of the condensed phase, two setups were used. The first setup was built around the cylindrical tight plasma reactor with an inner diameter of 14 cm and a height of 15 cm (a volume of 2.3 L) from aluminum alloy. Horizontally oriented steel cathode represented a massive plate placed under a vertically oriented graphite anode. The voltage on the electrodes was 27 V for an electric current in the arc equal to 45 A. The electrodes were placed on the axis of the plasma chemical reactor. The arc discharge plasma emission spectrum was recorded with the second setup without case.

The magnetic field with tangentially oriented lines was created around the electric discharge channel. In the presence of external permanent magnetic field, the total field decreased along the radius toward the center of the plasma channel and decayed to the external field at large distances from the center. Two magnetic field sources were used. Permanent magnets were oriented perpendicularly to the plasma channel. A magnetic field of 9.5 mT, created by the coil, stabilized the position of the arc. The axis of the coil, connected to the electric circuit of the arc, coincided with the axis of the electrode system.

The Ar – 3 %, O_2 – 18 %, and N_2 – 79 % (by volume) gas mixture was supplied at a flow rate of 0.6 l/min from cylinders through a nozzle at the bottom of the plasma reactor. After switching on the power supply unit, the electrodes were mechanically closed. They were subsequently moved apart at a distance of 5-6 mm under the action of a spring. The arc heated the graphite and steel electrodes that began to evaporate intensively 5–10 min after electric arc ignition. To investigate the dispersed powder by the x-ray diffraction method, it was collected from the inner walls of the plasma reactor. To perform SEM analysis, the powder was deposited on a glass substrate with aluminum coating placed horizontally at a distance of 15 mm from the arc perpendicular to the magnetic field lines of the permanent magnets. A part of the aerosol went through the slit with sizes of 2 × 60 mm located at the top of the cylinder on its periphery. This aerosol flow was sensed by broadband radiation. The transmitted radiation spectrum was recorded with an SL-140 small-sized spectrometer.

6. EXPERIMENTAL RESULTS

The emission spectra of the arc discharge plasma channel between the steel and graphite (curve *1*) and the graphite (curve *2*) electrodes are shown in Fig. 3*a*. We revealed no effect of the 15 mT magnetic field on the arc emission spectrum.

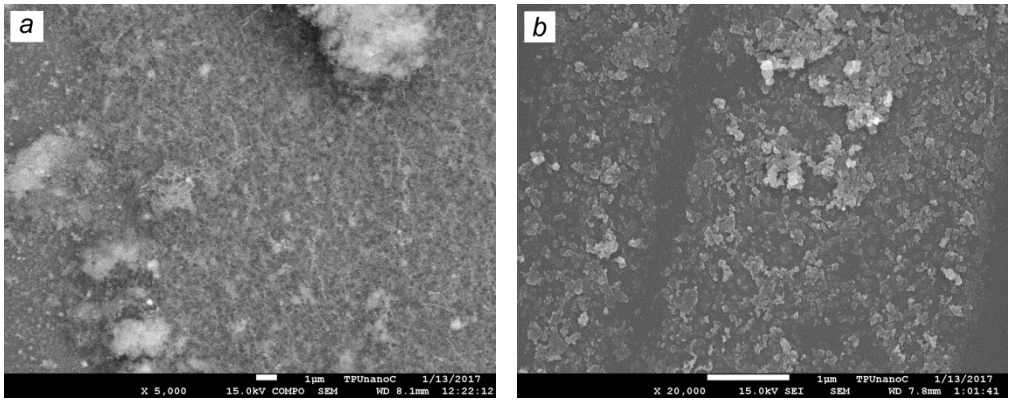

Fig. 4. SEM images of the powder formed from the arc plasma without (*a*) and with a magnetic field of 15 mT (*b*).

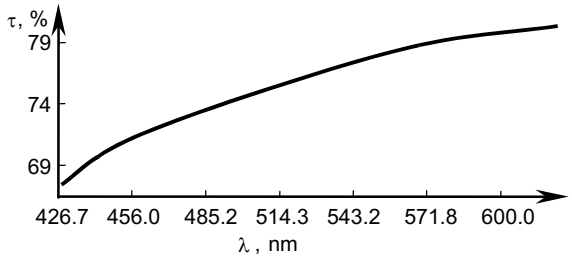

Fig. 5. Transmission spectrum of the powder formed from the arc discharge plasma without magnetic field.

The phase composition of the powder of brown color formed as a result of plasma processes and deposited on the walls was analyzed by the x-ray diffraction method using an XRD-7000S series diffractometer. Figure 3*b* shows one of the x-ray diffraction patterns of the powder formed in the reactor. In the powder formed without application of magnetic field, the x-ray diffraction analysis demonstrates the presence of up to 95 % of carbon. The iron oxides were observed in insignificant amounts. The data of x-ray diffraction analysis in an external permanent magnetic field of 10 mT demonstrated the presence of the dispersed phase in which the microcrystal content decreased in the sequence: C (to 50 %), Fe_3O_4 (to 45 %), Fe_2O_3 (to 15 %), and FeO (less than 5 %). Iron carbides in the dispersed phase were not detected.

Figure 4 shows SEM images of the powder formed in the arc discharge plasma channel and recorded with a JEOL JSM-7500FA series scanning electron microscope. Without magnetic field, volume conglomerates of the nanodispersed powder having arbitrary shapes and sizes up to 15 microns can be distinguished in the photomicrographs together with a certain amount of spherical particles with sizes less than 1 μm. In the presence of the magnetic field, spherical particles practically did not appear, and nanoparticle conglomerates were shaped as flakes whose sizes did not exceed 0.3 μm.

Figure 5 shows the transmission spectrum of the powder formed in the plasma reactor without magnetic field. The light-emitting diode with a long-wavelength converter was used as a radiation source. The image of the emitting plate was adjusted using a lens at the center of the nozzle forming aerosol flow during action of the arc discharge. The radiation transmission coefficient monotonically increased in the wavelength range 420–630 nm. A sharp decrease in the transmission coefficient at the ends of the wavelength range was caused by the decrease of the intensity of the light-emitting diode.

Using the data shown in Fig. 5, the inverse problem was solved. It was established that the best fit to the experimental data is provided by the size distribution function with particle diameters of 11–40 nm and the complex refractive index of the particle material $m = 2.3–i0.96$.

7. DISCUSSION OF EXPERIMENTAL RESULTS

The condensed products of the plasma processes were formed when the plasma forming gas arrived on the periphery of the discharge channel being cooled by a radial plasma expansion and a radial temperature gradient. The iron vapors and its oxides can condense on the carbon particle surfaces and on the new iron oxide nucleation centers in the vapor phase. Because of high cooling rate and liberation of the energy of phase transition, the sizes of crystals containing iron atoms (the specific heat of vaporization of iron is 6300 kJ/kg) were also limited.

From the three iron oxides, the mixed oxide (II, III), Fe_3O_4 (magnetite), and γ-Fe_2O_3 (maghemite) possess magnetic properties, and α-Fe_2O_3 (hematite) has weak antiferromagnetic properties. Without magnetic field, the probability of coagulation of dispersed particles $(FeO_x)_n$, determined by their diffusion at atmospheric pressure, is low. In the magnetic field, the FeO_x particles having magnetic moments were attracted along the lines of the magnetic field strength. In the magnetic field, the process of agglomeration of ferromagnetic particles with subsequent formation of a uniform crystal accelerated. The ratio of times of close approach of ferromagnetic particles via the magnetic and the Brown diffusion can be described by the formula [30]

$$\frac{t_{\rm m}}{t_{\rm d}} = \frac{0.67\,kT}{\mu_0 R_{\rm f}^5 H_0^2 \left(N_{\rm v0}\right)^{2/3}} \frac{\chi_{\rm fi} + 3}{\chi_{\rm fi}^2}. \qquad (12)$$

The field promotes the formation of larger $(FeO_x)_n$ particles before their collision with carbon particles, and also their merging on the carbon particle surface. The high temperature and liberation of the sublimation energy promoted the formation of a homogeneous crystal (annealing). Therefore, both graphite and iron oxide were recorded by the method of x-ray diffraction analysis of the powder in the presence of the magnetic field.

This suggests that the iron oxide microcrystals formed without magnetic field have much smaller sizes than the sizes that can be detected by the x-ray diffraction method. This can be due to the fact that the sizes of the iron oxide microcrystals were comparable with the x-ray radiation wavelength. The x-ray diffractometer used the Cu$K\alpha_1$ and Cu$K\alpha_2$ lines (1.54051 and 1.54433 Å) for the presented analysis.

A study of the SEM images of the CDP particles formed from the arc discharge containing Cu and SiO_2 vapors demonstrates that the dispersed particles formed without magnetic field and having sizes of 0.1–1.5 μm were surrounded by *friable* coatings from smaller particles. In the magnetic field, particles with sharp boundaries and sizes in the range 0.1–2.5μm were formed. In the magnetic field, the condensed phase was formed containing much less amount of particles of nanometer sizes than the phase formed without magnetic field.

The formation and growth of the nucleation centers of the condensed phase was identical for systems containing Fe or Cu atoms. The increase of the frequency of forming the condensation nuclei is caused by the increase in the probability of forming singlet spin pairs in the magnetic field. The particles containing Cu and SiO_2 did not interact ferromagnetically. In case of diamagnetic particles, the growth of the dispersed particles was strongly influenced by the dynamics of spin pairs on the surface between uncoupled valence electrons of the surface atoms and atoms of the vapor phase. In case of growth of the ferromagnetic particles in a magnetic field, the main contribution comes from the ferromagnetic interaction of already existing particles.

CONCLUSIONS

It has been established experimentally that the external magnetic field affects considerably the plasma processes of forming the dispersed phase upon cooling of the argon-oxygen plasma containing C and Fe atoms as well as Cu and SiO_2. In the above-indicated conditions, the dispersed particles were formed containing mechanical mixture

of microcrystals of the condensed substances in the form of oxides of the employed elements: C and Cu. The presence of FeO_x or SiO_2 oxides complicated heterogeneous reactions of C and Cu oxidation. Such processes allowed graphite depleted in the ^{13}C isotope and formed from the remaining isotope-selective plasma processes to be retained in its dispersed phase.

It was also established that in the external permanent magnetic field the dispersed particles formed from ferromagnetic and diamagnetic substances have large sizes and sharper boundaries than those formed without magnetic field. This demonstrates the effect of spin dynamics of uncoupled electrons of molecules that interact in the vapor phase and on the surface on the nucleation process.

When performing this work, the electron microscope of the TPU Nano-Center and the x-ray diffractometer of the Center for Collective Use at TPU were used.

This work was supported in part by the Russian Foundation for Basic Resarch (Grant No. 16-08-00246).

REFERENCES

1. V. F. Myshkin, V. A. Khan, V. G. Plekhanov, *et al*., Russ. Phys. J., **57**, No. 10, 1442–1448 (2015).
2. V. F. Myshkin, E. V. Bespala, V. A. Khan, *et al*., IOP Conf. Ser.: Mater. Sci. Eng., **135**, No. 1, 012029 (2016).
3. A. Gleizes, H. Kafrouni, H. Duc, and C Maury, J. Phys. D, **15**, 1031–1045 (1982).
4. S. P. Umnov and V. F. Myshkin, Phys. Chem. Mater. Treatm., **23**, No. 1, 39–42 (1989).
5. E. I. Karpenko, V. E. Messerle, B. G. Trusov, *et al*., Goren. Plazmokhim., **1**, No. 4, 291–310 (2003).
6. Ya. B. Zel'dovich, A. L. Buchachenko, and E. L. Frankevich, Usp. Fiz. Nauk, **155**, No. 1, 3–45 (1988).
7. H. David, McIntyre Spin and Quantum Measurement, Oregon State University (2002).
8. V. E. Fortov, A. G. Khrapak, and I. T. Yakubov, Nonideal Plasma Physics: A Textbook [in Russian], Fizmatlit, Moscow (2004).
9. B. M. Smirnov, Usp. Fiz. Nauk, **170**, No. 5, 495–534 (2000).
10. V. N. Smirnov, Kinet. Catal., **52**, 166–169 (2011).
11. V. N. Smirnov, Kinet. Catal., **53**, 543–553 (2012).
12. J. M. C. Plane, C. I. Whalley, L. Frances-Soriano, *et al*., J. Chem. Phys., **137**, 014310 (2012); DOI: 10.1063/1.4730423.
13. J. M. C. Plane and R. Rollason, J. Phys. Chem. Chem. Phys., **1**, No. 8, 1843 (1999).
14. M. Helmer and J. M. C. Plane, J. Chem. Soc. Faraday Trans., **90**, No. 3, 395 (1994).
15. A. R. Fairbairn, Proc. R. Soc. London A, **312**, 207–227 (1969).
16. E. Jans, K. Frederickson, M. Yukovich, *et al*., J. Chem. Phys. Lett., **659**, 112–116 (2016).
17. M. Laca, L. Schmiedt, V. Hrachova, and A. Kanka, in: WDS' 13 Proceedings of Contributed Papers, Part II, Prague (2013), pp. 120–126.
18. S. A. Lawton and A. V. Phelps, J. Chem. Phys., **69**, No. 3, 1055–1068 (1978).
19. A. M. Starik, B. I. Lukhovitskii, V. V. Naumov, and N. S. Titova, Zh. Tekh. Fiz., **77**, No. 10, 34–42 (2007).
20. V. M. Shopin, Zh. Ross. Khim. Obshch. Im. D. I. Mendeleeva, **60**, No. 4, 104–110 (2007).
21. K. D. Froyd and E. R. Lovejoy, J. Phys. Chem. A, **107**, No. 46, 9800–9811 (2003).
22. M. P. Anisimov, Usp. Khim., **72**, No. 7, 664–705 (2003).
23. V. A. Pavlov and V. P. Skripov, Teplofiz. Vysok. Temp., **8**, 579–585 (1976).
24. A. G. Amelin, Theoretical Bases of Fog Formation during Vapor Condensation [in Russian], Khimiya, Moscow (1972).
25. A. G. Gorelik and A. V. Amitin, Desublimation in Chemical Industry [in Russian], Khimiya, Moscow (1986).
26. R. Perekrestov, P Kudrna, M. Tichý, *et al*., J. Phys. D, **49**, 265201 (2016).
27. V. Stranak, A.-P. Herrendorf, H. Wulff, *et al*., Surf. Coat. Technol., **222**, 112–117 (2013).
28. B. M. Smirnov, Usp. Fiz. Nauk, **170**, No. 5, 495–534 (2000).
29. D. I. Zhukhovitskii, A. G. Khrapak, and I. T. Yakubov, Teplofiz. Vys. Temp., **22**, No. 5, 833–840 (1984).
30. E. M. Bulyzhev and E. N. Men'shov, Izv. Samarsk. Nauchn. Tsentra, **16**, No. 1, 247–254 (2014).